AIAA JOURNAL
Vol. 39, No. 7, July 2001

# Unsteady Forces on a Two-Dimensional Wing in Plunging and Pitching Motions

S. Sunada*
*Ministry of International Trade and Industry, Ibaraki 305-8564, Japan*
K. Kawachi† and A. Matsumoto‡
*University of Tokyo, Tokyo 153-8904, Japan*
and
A. Sakaguchi§
*Fuji Heavy Industries, Ltd., Tochigi 320-0834, Japan*

**Unsteady fluid dynamic forces acting on a two-dimensional wing in sinusoidal plunging and pitching motions in still water were measured. The measured fluid dynamic forces were larger than those estimated by quasi-steady analysis, where the effect of unsteady separated vortices on the fluid dynamic forces is not considered. Vortex capture is a phenomenon related to the larger fluid dynamic forces in wing motion that is similar to wing motion of real insects. By using the measured fluid dynamic forces, we identified combinations of plunging and pitching motions for maximum time-averaged thrust and for maximum efficiency.**

## Nomenclature

| | | |
|---|---|---|
| $a$ | = | dimensionless position of the rotational axis of the pitching motion |
| $b$ | = | span length of the wing immersed in water |
| $C_\ell$, $C_d$ | = | lift and drag coefficients |
| $C_n$, $C_t$ | = | normal and tangential force coefficients |
| $C_X$, $C_Z$ | = | force coefficients in $X$ and $Z$ directions |
| $c$ | = | chord length |
| $\boldsymbol{c}$ | = | chord vector |
| $F_n$, $F_t$ | = | fluid dynamic forces normal and tangential to airfoil chord |
| $F_X$, $F_Z$ | = | fluid dynamic forces in $X$ and $Z$ directions |
| $F_x$, $F_z$ | = | forces in $x$ and $z$ directions |
| $f$ | = | frequency of both pitching and plunging motions |
| $h$ | = | displacement of plunging motion |
| $h_a$ | = | amplitude of plunging motion |
| $k$ | = | reduced frequency |
| $L_X$, $L_Y$, $L_Z$ | = | size of the water tank |
| $M_x$, $M_y$, $M_z$ | = | moments around $x$, $y$, and $z$ axes |
| $\bar{P}$ | = | power |
| $Re$ | = | Reynolds number |
| $r$ | = | distance between 75% chordwise position and the rotational axis, expressed as Eq. (16) |
| $T$ | = | period of one cycle of motion |
| $t$ | = | time |
| $t/c$ | = | thickness ratio of wing |
| $U$ | = | uniform velocity |
| $\boldsymbol{V}_{\text{in}}$ | = | inflow velocity |
| $\bar{v}$ | = | time-averaged induced velocity |
| $X$, $Y$, $Z$ | = | orthogonal Cartesian system fixed on the water tank |
| $x$, $y$, $z$ | = | coordinate system fixed on the wing |
| $\alpha$ | = | pitching angle |
| $\alpha_r$ | = | angle between $\boldsymbol{c}$ and $\boldsymbol{V}_{\text{in}}$ |
| $\alpha_0$ | = | mean pitching angle |
| $\alpha_1$ | = | amplitude of pitching motion |
| $\tilde{\alpha}$ | = | instantaneous angle of attack, expressed in Eq. (18) |
| $\Delta$ | = | error |
| $\eta$ | = | efficiency |
| $\nu$ | = | kinematic viscosity |
| $\rho$ | = | density |
| $\phi$ | = | phase difference between plunging and pitching motions |
| $\bar{\phi}$ | = | value of $\phi$ |
| $\bar{\ }$ | = | time-averaged value |
| $\tilde{\ }$ | = | force or moment acting on a load cell |

*Subscripts*

| | | |
|---|---|---|
| $A$ | = | forces due to added mass |
| $C$ | = | circulatory forces |
| qs | = | values determined by quasi-steady analysis |

## Introduction

IT was first proposed by Weis-Fogh[1] that certain insects generate larger fluid dynamic forces in hovering flight than those estimated by quasi-steady analysis.[2] (Quasi-steady analysis is based on the potential flow theory, where the unsteady effect on the wing circulation is ignored.) Later research justified Weis-Fogh's hypothesis about the flight of real insects.[3–5] Furthermore, studies involving three-dimensional or two-dimensional model wings were done to clarify the mechanism that generates these large fluid dynamic forces. Two such studies involving three-dimensional flapping wings were by Ellington et al.[6] and by Dickinson.[7] Ellington et al.[6] did flow visualization for a three-dimensional flapping wing and found that the spanwise flow stabilizes the leading-edge vortices, causing high lift. Dickinson[7] measured the instantaneous fluid dynamic forces acting on a three-dimensional flapping wing and explained that the large fluid dynamic forces are due to three phenomena: 1) delayed stall, 2) rotational circulation, and 3) wake capture.

In three-dimensional flapping wings, a wing section (blade element) parallel to a flapping axis makes plunging and pitching motions. Studies involving two-dimensional wings undergoing such motions were conducted by Dickinson and Götz,[8] Dickinson,[9] Freymuth,[10] Gustafson and Leben,[11] and Gustafson et al.[12,13] Note that the two-dimensional wings correspond to a wing section in the three-dimensional flapping wing. The fluid dynamic forces obtained

Received 10 June 2000; revision received 29 September 2000; accepted for publication 29 December 2000. 

*Senior Researcher, Department of Advanced Machinery, Mechanical Engineering Laboratory; sunada@mel.go.jp.
†Professor, Research Center for Advanced Science and Technology. Associate Fellow AIAA.
‡Graduate Student, Research Center for Advanced Science and Technology.
§Engineer, Aerospace Division.

in these studies were larger than those estimated by quasi-steady analysis. Dickinson and Götz[8] measured the instantaneous fluid dynamic forces acting on a two-dimensional wing just after an impulsive start. The cause for high lift in this wing motion is delayed stall and vortex capture. Dickinson[9] also measured the instantaneous fluid dynamic forces acting on an impulsively started two-dimensional wing just after rotational motion. The main cause for high lift in this wing motion is wake capture, when the wing translates backward through a wake generated by the previous stroke. Freymuth[10] studied a wing undergoing sinusoidal plunging and pitching motions. He measured the velocity field around the wing by using pitot tubes and then determined the time-averaged thrust by combining the measured velocity distribution with simple momentum theory. In addition, he visualized the flow around the wing by using a titanium–tetra–chloride method.[14] Using computational fluid dynamics analysis, Gustafson and Leben[11] and Gustafson et al.[12,13] confirmed that the time-averaged thrust generated by a wing undergoing sinusoidal plunging and pitching motions is larger than that calculated by quasi-steady analysis. The studies by Freymuth,[10] Gustafson and Leben,[11] and Gustafson et al.[12,13] provide no details of the instantaneous fluid dynamic force.

In our experiments, we used a load cell with strain gauges to measure directly the instantaneous forces acting on a wing undergoing a plunging motion coupled with a pitching motion. By using the measured fluid dynamic forces, we identified the combinations of these two motions for maximum time-averaged thrust and for maximum efficiency. In addition, we did flow visualization to understand the relation between the flow around a wing and the fluid dynamic force acting on the wing.

## Experimental Apparatus and Procedure

### Measurement System

Figures 1a and 1c show top and side views of the experimental apparatus, and Fig. 1b shows the top view of the wing. The measurement system included a wing, a water tank, two servomotors (A and B), a load cell (LMC 3729-1N; Nissho Electric Works), two strain amplifiers (one each for the two components of forces, $F_x$ and $F_z$), and two computers. One computer controlled two servomotors A and B, and the other collected the signals indicating the time variation in the forces measured by the load cell and two strain amplifiers.

In the water tank, the wing moved in a combination of plunging and pitching motions. The pitching motion was generated by servomotor A, whose axis was parallel to the rotation axis of the pitching motion. Pitching angle is defined in Fig. 1b.

The plunging motion was generated by servomotor B. When servomotor B in tower 2 rotated plate 2 around the axis of servomotor B, the following motions occurred: 1) The plunging table slid in the $X$ direction. 2) Rod 3, which was connected perpendicularly to plate 2, rotated around the axis of servomotor B. 3) Rod 2, which was connected to rod 3 via a joint, and plate 1 rotated around rod 1, which was connected perpendicularly to plate 1 via a bearing. When the angular velocity of servomotor B was constant, the plunging motion was perfectly sinusoidal.

The wing we used had a rectangular airfoil section (Fig. 2) in which the chord length $c$ was 28.3 mm, the thickness ratio $t/c$ was 5%, and the span length was 300 mm. The rotation axis of the pitching motion was located at $x = a(c/2)$. The value of $a$ was $-0.5$ and 0 when the rotation axis of the pitching motion was at the 25 and 50% chordwise position, respectively. The wing was immersed to a depth $b$ of 280 mm in the water tank, with part of the wing remaining above the water surface.

The size of the water tank was $L_X = L_Z \simeq 3000$ mm $\simeq 75h_a$, where $h_a$ is the amplitude of the plunging motion as indicated by Eq. (1), and $L_Y \simeq 360$ mm $\simeq 1.3b$, where $b$ is the span length of the wing immersed in the water. The values of $L_X/h_a = L_Z/h_a$ and $L_Y/b$ were sufficiently large so that the wall effect of the tank could be ignored. The value for $b/c \simeq 10$ was sufficiently large so that we assumed (assumption 1) that both the three-dimensional effect due to the finite value of $b/c$ on the fluid dynamic forces acting on the wing and the effect of the wave on the water surface on these forces were relatively small and, therefore, could be ignored.

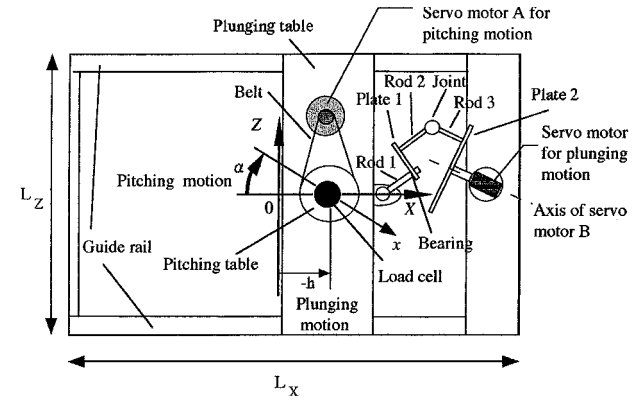


a) Top view

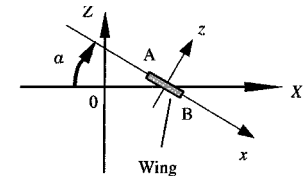


b) Top view of wing

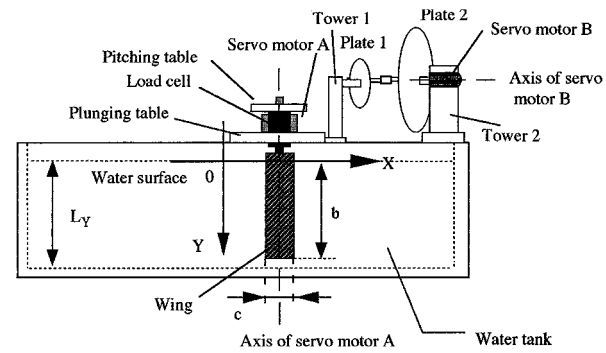


c) Side view

**Fig. 1 Apparatus used to measure the fluid dynamic force of a two-dimensional wing undergoing plunging and pitching motions.**

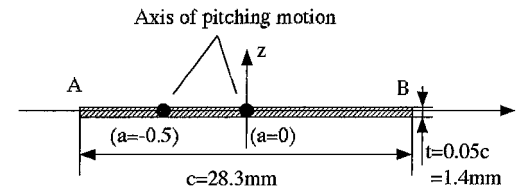


**Fig. 2 Wing-section shape.**

The load cell can measure $F_x$, $F_z$, and $M_y$. The output signals of $F_x$, $F_z$, and $M_y$ from the load cell are determined by the five components of forces and moments acting on the load cell, that is, $\tilde{F}_x$, $\tilde{F}_z$, $\tilde{M}_x$, $\tilde{M}_y$, and $\tilde{M}_z$. However, the output signals of $F_x$ and $F_z$ were nearly equal to the forces acting on the load cell, $\tilde{F}_x$ and $\tilde{F}_z$, respectively.

The load cell and two strain amplifiers with a low-pass filter, whose cutoff frequency was 1 Hz, were used to measure the fluid dynamic forces on the wing. This measurement system caused a time delay between the real fluid dynamic forces and their measured values. We have compensated for this time delay.

The forces measured by this system consisted of the fluid dynamic normal force in the $z$ direction, $F_n$, tangential force in the $x$ direction, $F_t$, and inertial normal and tangential forces resulting from the motion of the wing. The inertial forces of the wing moving through the water were directly measured in the same manner used for the wing moving through air because the inertial forces

in air were much larger than the fluid dynamic forces in air. We determined $F_n$ and $F_t$ by subtracting the inertial forces measured in air from the forces measured in water.

**Flow Visualization**

Aluminum dust was sprinkled over the water surface to make the flow patterns around the wing visible on the water surface.

**Reynolds Number and Reduced Frequency**

The motion of the wing consisted of both a plunging motion $h$ in the $-X$ direction and a pitching motion $\alpha$ about the rotation axis and is expressed as

$$h = h_a \sin(2\pi f t), \qquad \alpha = \alpha_0 + \alpha_1 \sin(2\pi f t + \phi) \tag{1}$$

Table 1 lists the values of these parameters used in our measurements.

We measured the periodic force after about 1 min (12 cycles) of wing motion. The Reynolds number $Re$ and reduced frequency $k$ are based on $c$, $f$, and the maximum plunge speed $2\pi f h_a$ and are expressed by

$$Re = 2\pi f h_a c/\nu = 10^3$$
$$k = (2\pi f)c/2(2\pi f h_a) = c/2h_a = 0.35 \tag{2}$$

These values of $Re$ and $k$ agree well with those in the hovering flight of a dragonfly.[15] The $k$ is determined here only by the chord length $c$ and the amplitude of plunging motion $h_a$ and not by frequency $f$. However, $k$ indicates an unsteady effect of wing motion on fluid dynamic force acting on a wing as follows. Because the bound vortices distribute evenly on the airfoil, the length of the bound vortex sheet is given by $c$, and the length of the shed vortex sheet generated during one cycle of motion is $2h_a$. Therefore, the ratio between $c$ and $h_a$ represents the interference effect between the bound vortices and the shed vortices. This interference effect is the unsteady effect of wing motion on the fluid dynamic forces acting on the wing. Note that the reduced frequency for a wing during unsteady motion in uniform flow,[2] $k = \pi f c/U$, also indicates the ratio between the chord length $c$ and the length of the shed vortex sheet generated during one cycle of wing motion, $U/f$.

**Instantaneous Fluid Dynamic Force Coefficients**

The instantaneous force coefficients $C_Z$ and $C_X$ are obtained by nondimensionalizing the total fluid dynamic forces in the $Z$ and $X$ directions, $F_Z$ and $F_X$, by a constant force $\rho(\pi f h_a)^2 bc$ as follows:

$$C_Z = F_Z/\rho(\pi f h_a)^2 bc = (F_n \cos\alpha - F_t \sin\alpha)/\rho(\pi f h_a)^2 bc \tag{3}$$

$$C_X = F_X/\rho(\pi f h_a)^2 bc = (F_n \sin\alpha + F_t \cos\alpha)/\rho(\pi f h_a)^2 bc \tag{4}$$

**Table 1 Wing-motion parameters**

| Parameter | Value |
|---|---|
| $f$, 1/s | $1.2/2\pi(=0.19)$ |
| $h_a$, mm | $40(=1.4c)$ |
| $\alpha_0$, deg | 0, 30, 60, 90 |
| $\alpha_1$, deg | 30, 60, 90 |
| $\phi$, deg | 0, 45, 90, 135, −45, −90, −135, −180 |
| $a$ | 0, −0.5 |

For comparison with those values obtained by Freymuth,[10] as defined later [Eq. (5)], these time-averaged values were nondimensionalized by using the mean square velocity.

**Time-Averaged Force Coefficients**

The time-averaged force coefficients $\bar{C}_Z$ and $\bar{C}_X$ are

$$\bar{C}_Z = \frac{1}{T}\int_0^T C_Z \,\mathrm{d}t, \qquad \bar{C}_X = \frac{1}{T}\int_0^T C_X \,\mathrm{d}t, \qquad T = \frac{1}{f} \tag{5}$$

where $\bar{C}_Z$ corresponds to $C_T$ used by Freymuth.[10]

**Efficiency**

In accord with to simple momentum theory,[16] the time-averaged induced velocity in the $-Z$ direction, $\bar{v}$, is given by

$$\bar{v} = \frac{\bar{F}_Z}{2|\bar{F}_Z|}\sqrt{\frac{|\bar{F}_Z|}{\rho h_a b}} \tag{6}$$

Efficiency $\eta$ is given by

$$\eta = \frac{\bar{F}_Z \bar{v}}{\bar{P}} = \frac{|\bar{F}_Z|^{1.5}}{2\sqrt{\rho h_a b}\,\bar{P}} \tag{7}$$

where $\bar{P}$ is the power required for a plunging motion and is given by

$$\bar{P} \simeq \left(\frac{1}{T}\right)\int_0^T \dot{h} F_X \,\mathrm{d}t \tag{8}$$

This equation assumes (assumption 2) that the power required for pitching motion is much smaller than that for plunging motion and, thus, can be ignored.

**Relation of $\bar{C}_Z$ and $\eta$ Between Symmetrical Wing Motions**

When $a = 0$ or when $\alpha_0 = 0$, the wing motions of $\phi = \bar{\phi}$ are symmetrical to those of $\phi = \bar{\phi} \pm 180$ deg about point $O$. Therefore, Eqs. (26) and (27) in Table 2 are satisfied.

The pitching axis was located at the 50% ($a = 0$) or 25% ($a = -0.5$) chordwise position, as stated earlier. The fluid dynamic forces in the wing motion for $a = 0.5$, when a pitching axis is located at 75% chordwise position, can be estimated from those for $a = -0.5$ by using Eqs. (28) in Table 2. These equations are obtained from the symmetry between the wing motions of $a = 0.5$ and $\phi = \bar{\phi}$ and those of $a = -0.5$ and $\phi = \bar{\phi} \pm 180$ deg about point $O$.

**Quasi-Steady Analysis**

Here we discuss the application of quasi-steady analysis based on linear theory for an unsteady wing[2] to our present experiments. Note that the effect of separated vortices on fluid dynamic forces is not considered in this quasi-steady analysis.

In quasi-steady analysis, the fluid dynamic forces acting on a wing, $F_{Z,\mathrm{qs}}$ and $F_{X,\mathrm{qs}}$, are composed of noncirculatory forces due to added mass, $F_{Z,A}$ and $F_{X,A}$, and circulatory forces due to circulation of a wing, $F_{Z,C}$ and $F_{X,C}$, as follows:

$$F_{Z,\mathrm{qs}} = F_{Z,A} + F_{Z,C}, \qquad F_{X,\mathrm{qs}} = F_{X,A} + F_{X,C} \tag{9}$$

*Noncirculatory Forces Due to Added Mass*

The theoretical normal force due to added mass acting on a two-dimensional wing with zero thickness[17] is

$$F_{n,A} = 0.25\pi\rho bc^2(\ddot{h}\sin\alpha + \dot{h}\cos\alpha\dot{\alpha} - 0.5ac\ddot{\alpha}) \tag{10}$$

**Table 2 Relations of $\bar{C}_Z$ and $\eta$ between the symmetrical wing motions**

| $\alpha_0$ | $a$ | $\bar{C}_Z(a,\phi)$, $\eta(a,\phi)$ | Equation |
|---|---|---|---|
| Any value | 0 | $\bar{C}_Z(a=0,\phi=\bar{\phi}) = -\bar{C}_Z(a=0,\phi=\bar{\phi}\pm 180\text{ deg})$<br>$\eta(a=0,\phi=\bar{\phi}) = \eta(a=0,\phi=\bar{\phi}\pm 180\text{ deg})$ | (26) |
| 0 | Any value | $\bar{C}_Z(a,\phi=\bar{\phi}) = -\bar{C}_Z(a,\phi=\bar{\phi}\pm 180\text{ deg})$<br>$\eta(a,\phi=\bar{\phi}) = \eta(a,\phi=\bar{\phi}\pm 180\text{deg})$ | (27) |
| Any value | Values as indicated in Eqs. (28) | $\bar{C}_Z(a=0.5,\phi=\bar{\phi}) = -\bar{C}_Z(a=-0.5,\phi=\bar{\phi}\pm 180\text{ deg})$<br>$\eta(a=0.5,\phi=\bar{\phi}) = \eta(a=-0.5,\phi=\bar{\phi}\pm 180\text{ deg})$ | (28) |

The instantaneous forces due to the added mass on a two-dimensional wing with $t/c = 0.05$ in the $Z$ and $X$ directions are approximated by

$$F_{Z,A} = F_{n,A}\cos\alpha, \qquad F_{X,A} = F_{n,A}\sin\alpha \tag{11}$$

These forces are nondimensionalized by the constant force $\rho(\pi f h_a)^2 bc$ in the $Z$ and $X$ directions, and the coefficients for the fluid dynamic forces due to added mass are defined as

$$C_{Z,A} = F_{Z,A}/\rho(\pi f h_a)^2 bc = (0.25/\pi)\left\{c\Big/(f h_a)^2\right\}\cos\alpha(\ddot{h}\sin\alpha + \dot{h}\cos\alpha\dot{\alpha} - 0.5ac\ddot{\alpha}) \tag{12}$$

$$C_{X,A} = F_{X,A}/\rho(\pi f h_a)^2 bc = (0.25/\pi)\left\{c\Big/(f h_a)^2\right\}\sin\alpha(\ddot{h}\sin\alpha + \dot{h}\cos\alpha\dot{\alpha} - 0.5ac\ddot{\alpha}) \tag{13}$$

The time-averaged value of $C_{Z,A}$ is given by

$$\bar{C}_{Z,A} = \frac{1}{T}\int_0^T C_{Z,A}\,\mathrm{d}t \tag{14}$$

*Circulatory Forces Due to Circulation of Wing*

In linear theory, circulation of a two-dimensional wing is determined by inflow velocity at the 75% chordwise position, $\boldsymbol{V}_{\text{in}}$. The inflow velocity $\boldsymbol{V}_{\text{in}}$ in the $X$–$Z$ coordinate system is composed of the velocity due to wing motion and the induced velocity $\bar{v}$ and is given by

$$\boldsymbol{V}_{\text{in}} = (\dot{h} + rc\dot{\alpha}\sin\alpha, -\bar{v} + rc\dot{\alpha}\cos\alpha) \tag{15}$$

where $r$ is the distance between the 75% chordwise position and the rotational axis $x = a(c/2)$ and for cases when edge A is a leading edge is given by

$$r = -0.5a + 0.25 \tag{16a}$$

and for cases when edge B is a leading edge is given by

$$r = -0.5a - 0.25 \tag{16b}$$

For $\boldsymbol{V}_{\text{in}}$, the circulatory forces due to circulation of a wing $F_{Z,C}$ and $F_{X,C}$ are given by

$$F_{Z,C} = 0.5\rho|\boldsymbol{V}_{\text{in}}|^2 bc[C_\ell(\tilde{\alpha})\cos(\tilde{\alpha}) - C_d(\tilde{\alpha})\sin(\tilde{\alpha})]$$

$$F_{X,C} = 0.5\rho|\boldsymbol{V}_{\text{in}}|^2 bc[C_\ell(\tilde{\alpha})\sin(\tilde{\alpha}) + C_d(\tilde{\alpha})\cos(\tilde{\alpha})] \tag{17}$$

where $C_\ell(\tilde{\alpha})$ and $C_d(\tilde{\alpha})$ are lift and drag coefficients, respectively, which are defined for a wing moving at a constant velocity for a fixed angle of attack $\tilde{\alpha}$. Values for these coefficients are shown in Fig. A1 in the Appendix. The angle of $\tilde{\alpha}$ corresponds to the instantaneous angle of attack of the wing at the 75% chordwise position and is given by

$$\tilde{\alpha} = \alpha - \alpha_r = \alpha - \cos^{-1}\frac{(\boldsymbol{c}, \boldsymbol{V}_{\text{in}})}{|\boldsymbol{c}||\boldsymbol{V}_{\text{in}}|} \tag{18}$$

where $\boldsymbol{c}$ is a chord vector from edge B toward edge A. The circulatory fluid dynamic forces $F_{Z,C}$ and $F_{X,C}$ are nondimensionalized by the constant force $\rho(\pi f h_a)^2 bc$, and the coefficients are defined as follows:

$$C_{Z,C} = F_{Z,C}/\rho(\pi f h_a)^2 bc, \qquad C_{X,C} = F_{X,C}/\rho(\pi f h_a)^2 bc \tag{19}$$

In quasi-steady analysis, the fluid dynamic forces $F_{Z,\text{qs}}$ and $F_{X,\text{qs}}$ are obtained by using Eqs. (9–11) and Eqs. (15–18), respectively, and are nondimensionalized by the constant force $\rho(\pi f h_a)^2 bc$ as follows:

$$C_{Z,\text{qs}} = F_{Z,\text{qs}}/\rho(\pi f h_a)^2 bc = C_{Z,C} + C_{Z,A}$$

$$C_{X,\text{qs}} = F_{X,\text{qs}}/\rho(\pi f h_a)^2 bc = C_{Z,C} + C_{Z,A} \tag{20}$$

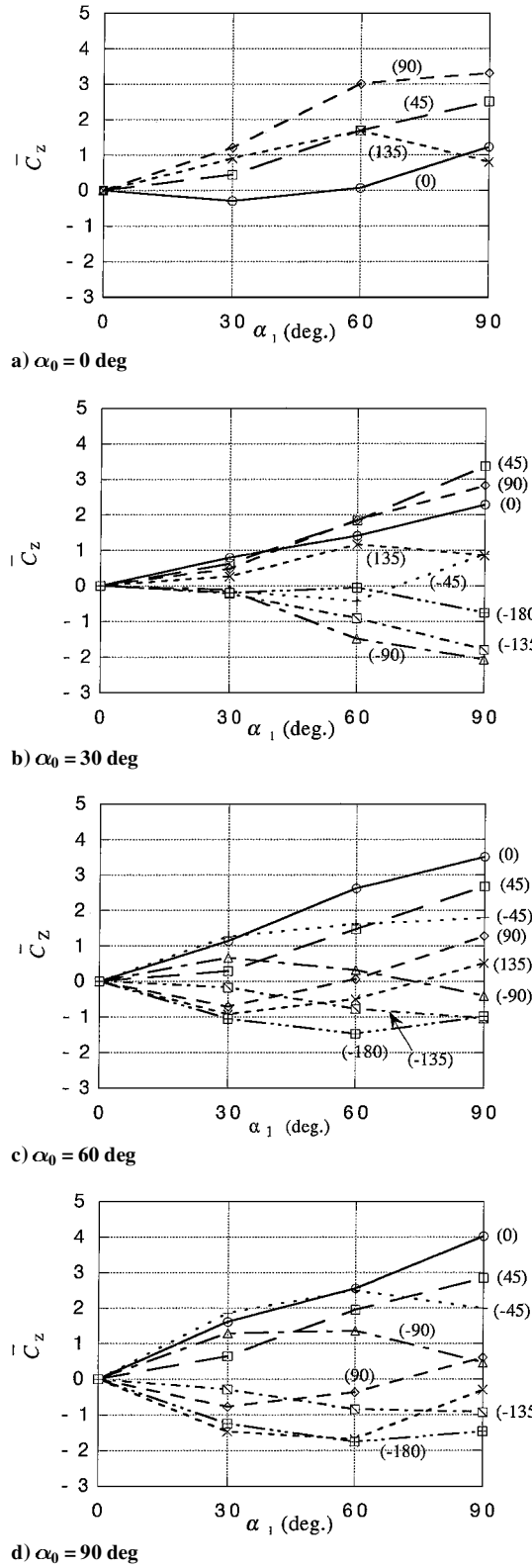


**Fig. 3 Time-averaged thrust coefficient $\bar{C}_Z$ for $a = -0.5$. (Values in brackets are the values of $\phi$.)**

The time-averaged force coefficients $\bar{C}_{Z,\text{qs}}$ and $\bar{C}_{X,\text{qs}}$ are

$$\bar{C}_{Z,\text{qs}} = \frac{1}{T}\int_0^T C_{Z,\text{qs}}\,\mathrm{d}t, \qquad \bar{C}_{X,\text{qs}} = \frac{1}{T}\int_0^T C_{X,\text{qs}}\,\mathrm{d}t \tag{21}$$

We compared coefficients $C_{Z,\text{qs}}$ and $C_{X,\text{qs}}$ with those obtained from our present measurements, $C_Z$ and $C_X$, respectively. The difference between $C_Z$ and $C_{Z,\text{qs}}$ or that between $C_X$ and $C_{X,\text{qs}}$ indicate the reliability of the quasi-steady analysis for the wing motions studied here.

**Experimental Uncertainty**

When measurements were repeated about a wing motion, the scatter in the data for measured $C_n$ and $C_t$ was $\Delta C_n$ and $\Delta C_t$, respectively. The maximum scatter was about $\pm 0.2$, thus causing an error $\Delta \bar{C}_Z$ in $\bar{C}_Z$. In all of our measurements, $\Delta \bar{C}_Z$ was less than 0.25:

$$\Delta \bar{C}_Z = \left| \frac{1}{T} \int_0^T (\pm \Delta C_n \sin\alpha \pm \Delta C_t \cos\alpha)\, dt \right| < 0.25 \qquad (22)$$

When this value of $\Delta \bar{C}_Z (< 0.25)$ is compared to the values of $\bar{C}_Z$ shown in Figs. 3, $\Delta \bar{C}_Z$ is much less than $\bar{C}_Z$ for a lot of wing motions. Therefore, the $\Delta \bar{C}_Z$ does not affect the conclusions stated later about $\bar{C}_Z$.

We estimated the error in $\Delta\eta/\eta$ caused by $\Delta C_n$ and/or $\Delta C_t$ as follows:

$$\frac{\Delta\eta}{\eta} = \left\{ 1 + \int_0^T \frac{(\pm \Delta C_n \cos\alpha \pm \Delta C_t \sin\alpha)}{(C_n \cos\alpha - C_t \sin\alpha)}\, dt \right\}^{1.5} \Bigg/ \left\{ 1 + \int_0^T \frac{\dot{h}(\pm \Delta C_n \sin\alpha \pm \Delta C_t \cos\alpha)}{\dot{h}(C_n \sin\alpha + C_t \cos\alpha)}\, dt \right\} \qquad (23)$$

We estimated $\eta$ by assuming an error $\Delta\eta/\eta < 0.25$, except when $\alpha_0 = \alpha_1 = 90$ deg and $\phi = \pm 90$ deg.

## Results and Discussion

The time-averaged thrust coefficient $\bar{C}_Z$ when $a = -0.5$ is shown in Figs. 3. For conciseness, only the results for $\phi = 0$, 45, 90, and 135 deg are shown in Fig. 3a. The results for $\phi < 0$ can be obtained from the preceding results by using Eqs. (26) and (27) (Table 2). For conciseness, $\bar{C}_Z$ when $a = 0$ are not shown.

The $\bar{C}_Z$ was maximum (about 4) for the wing motion where $a = -0.5$, $\alpha_0 = \alpha_1 = 90$ deg, and $\phi = 0$ deg. Efficiency for this wing motion is also fairly high ($\eta \simeq 0.8$), as shown later. Such efficiency makes this motion relevant to the development of small-scale fluid machinery.

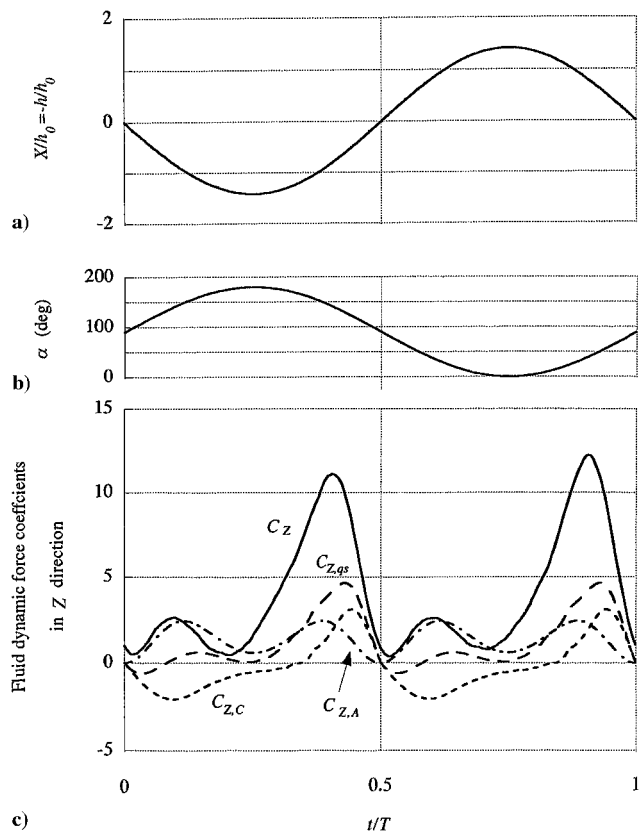


**Fig. 4 Maximum time-averaged thrust ($a = -0.5$, $\alpha_0 = \alpha_1 = 90$ deg, $\phi = 0$ deg): a) time variation of $X/h_0 = -h/h_0$, b) time variation of $\alpha$, and c) time variation of fluid dynamic force coefficients in the Z direction, $C_Z$, $C_{Z,A}$, $C_{Z,C}$, and $C_{Z,qs}$.**

In this wing motion, the time variations of $X/h_0 = -h/h_0$ and $\alpha$ and those of $C_Z$, $C_{Z,A}$, $C_{Z,C}$, and $C_{Z,qs}$ are shown in Figs. 4a, 4b, and 4c, respectively. Figure 4c shows that the measured value $C_Z$ is much larger than the quasi-steady estimation $C_{Z,qs} (= C_{Z,C} + C_{Z,A})$. Therefore, quasi-steady analysis cannot explain our measurement results obtained for this wing motion.

The efficiency $\eta$ when $a = -0.5$ is shown in Fig. 5. For conciseness, only the results for $\phi = 0$, 45, 90, and 135 deg are shown in Fig. 5a. The results for $\phi < 0$ can be obtained from the preceding

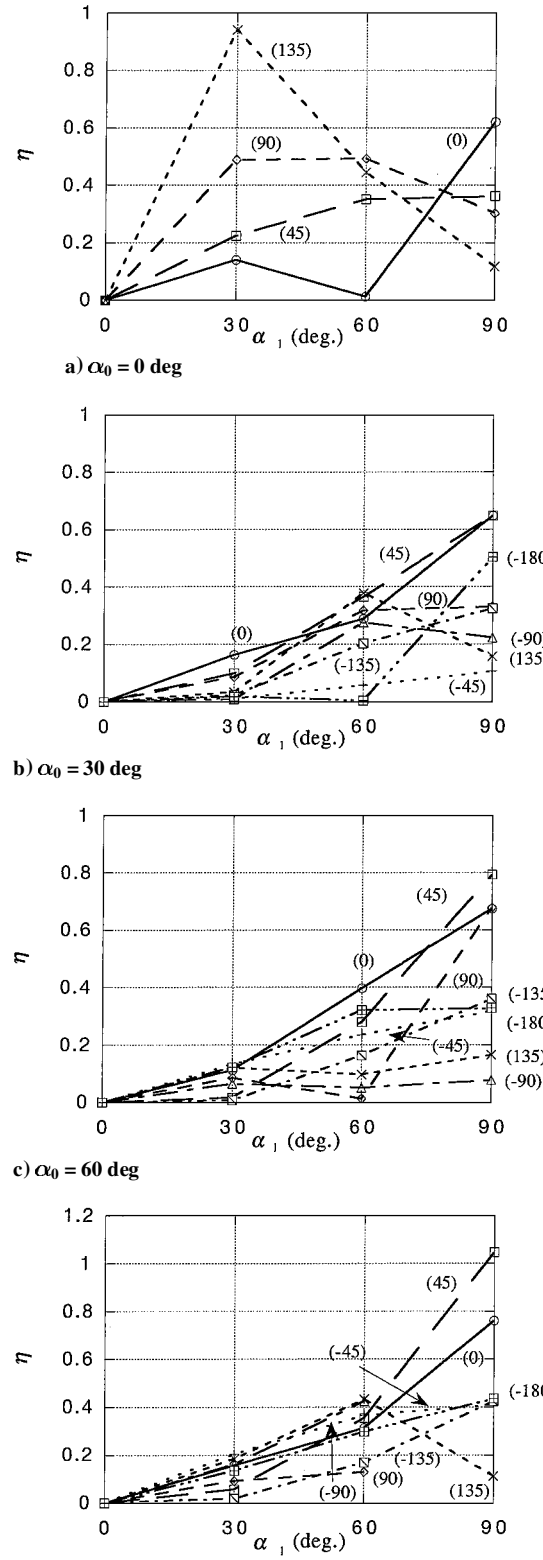


**Fig. 5 Efficiency $\eta$ for $a = -0.5$. (Values in brackets are the values of $\phi$.)**

results by using Eqs. (26) and (27) (Table 2). For conciseness, $\eta$ when $a = 0$ are not shown.

The $\eta$ was maximum (about 1) for the wing motion where $a = -0.5$, $\alpha_0 = \alpha_1 = 90$ deg, and $\phi = 45$ deg. Note that the efficiency $\eta$ was calculated under assumption 2 and that the values of $\eta$ probably decrease when the power consumed for pitching motion is also taken into account. The $\bar{C}_Z$ for this wing motion is about 2.8, as shown in Fig. 3d. This value is not small compared with those for the other motions shown in Figs. 3. Both the $\bar{C}_Z$ and $\eta$ for this wing motion are fairly high, and therefore, this wing motion can be used in small-scale fluid machinery.

Here, the wing motions for $\alpha_0 = \alpha_1 = 90$ deg and $\phi = \pm 90$ deg were excluded because the efficiency could not be estimated with high accuracy. However, the exclusion of these wing motions is not a serious problem because these motions, whose time-averaged thrust is small ($\bar{C}_Z \simeq 0.5$) as shown in Fig. 3d, are not relevant to small-scale fluid machinery.

For the wing motion, where $a = -0.5$, $\alpha_0 = \alpha_1 = 90$ deg, and $\phi = 45$ deg, for the maximum efficiency, the time variations of $\alpha$, those of $C_Z$, $C_{Z,A}$, $C_{Z,C}$, and $C_{Z,qs}$, and those of $C_X$, $C_{X,A}$, $C_{X,C}$, and $C_{X,qs}$, are shown in Figs. 6a, 6b, and 6c, respectively. The time variation of $X/h_0 = -h/h_0$ for this wing motion is shown in Fig. 4a. The time variation of $C_{X,C}$ has kinks at about $t/T \simeq 0.37$ and 0.87, as shown in Fig. 6c. The reason for these kinks is as follows. At these moments, the pitching angle $\alpha$ is 0, and the leading edge changes from edge A to edge B. The value of $r$ in Eq. (16), that is, the inflow velocity $\boldsymbol{V}_{\text{in}}$ in Eq. (15), abruptly changes at these moments. This abrupt change causes the kinks of the time variation of $F_{X,C}$ calculated by Eq. (17). At these moments, the sign of the values of $F_{Z,C}$ changes, and the values of $|F_{Z,C}|$ are smaller than those at the other moments. Therefore, the kinks in $F_{Z,C}$ are not evident at the moments in Fig. 6c.

In Figs. 6b and 6c, the discrepancy between $C_{Z,qs} (= C_{Z,A} + C_{Z,C})$ and $C_Z$ and that between $C_{X,qs} (= C_{X,A} + C_{X,C})$ and $C_X$ show that quasi-steady analysis cannot explain our measurement results obtained for this wing motion. In contrast, similarity exists between $C_{Z,A}$ and $C_Z$, (Fig. 6b), and between $C_{X,A}$ and $C_X$ (Fig. 6c), when $0 < t/T < 0.1$, $0.4 < t/T < 0.6$, and $0.9 < t/T < 1$. The fluid dynamic forces due to added mass, $C_{Z,A}$ and $C_{X,A}$, might be the dominant forces acting on the wing in this motion when $0 < t/T < 0.1$, $0.4 < t/T < 0.6$, and $0.9 < t/T < 1$. This dominance makes $\bar{P}$ smaller and, as a result, $\eta$ higher because power $\bar{P}$ is calculated from $F_X$ and $\dot{h}$, as indicated by Eq. (8), and because $F_{X,A}$ is nearly proportional to $\dot{h}$, as indicated by Eqs. (10) and (11). Note that

$$\left(\frac{1}{T}\right)\int_0^T \dot{h}\ddot{h}\,dt = 0$$

The comparison among our results, experimental results by Freymuth,[10] and numerical results by Gustafson et al.[12,13] for the time-averaged thrust coefficient $\bar{C}_Z$ is shown in Fig. 7a for $\alpha_0 = 0$ deg, $\phi = 90$ deg, and $a = 0$ and in Fig. 7b for $\alpha_0 = 90$ deg, $\phi = 90$ deg, and $a = 0$. Clear differences are observed in Fig. 7. The differences in parameters among the three methods used in the three respective studies are shown in Table 3. Freymuth[10] and Gustafson et al.[12,13] used a Reynolds number of $1.7 \times 10^3$ and a reduced frequency $k = c/2h_a$ of 0.33, differing slightly from the values we used in this study ($10^3$ and 0.35, respectively). Furthermore, the airfoil shapes, the averaged thickness of the wings, and the planform of the wings differed among all three methods. However, the differences in $\bar{C}_Z$ among the three methods, especially the differences seen in Fig. 7b, are thought to be too large to be explained by these differences in parameters among the three methods in Table 3. Reasons for these differences in the results among these studies are not yet clear.

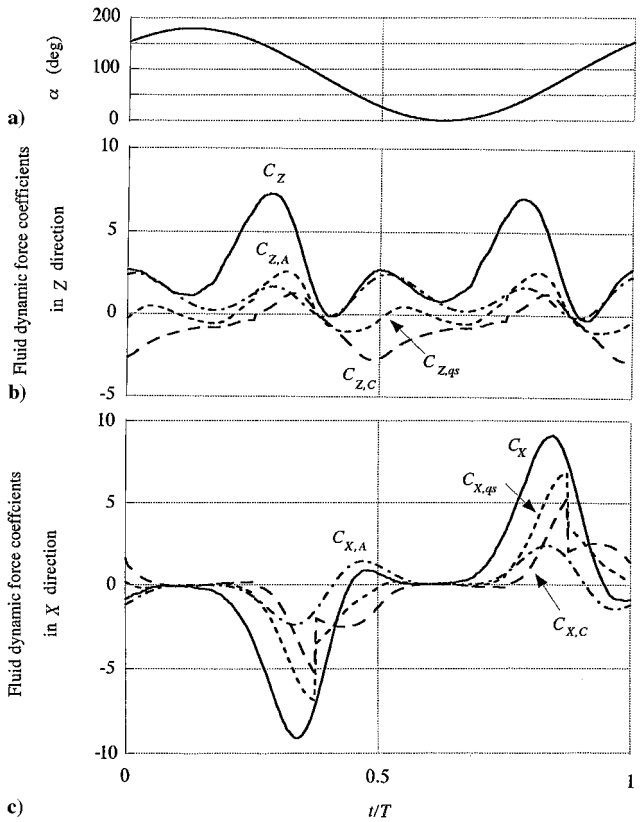


**Fig. 6 Maximum efficiency $\eta$ ($a = -0.5$, $\alpha_0 = \alpha_1 = 90$ deg, $\phi = 45$ deg): a) time variation of $\alpha$, b) time variations of fluid dynamic force coefficients in the Z direction, $C_Z$, $C_{Z,A}$, $C_{Z,C}$, and $C_{Z,qs}$, and c) time variations of fluid dynamic force coefficients in the X direction, $C_X$, $C_{X,A}$, $C_{X,C}$, and $C_{X,qs}$.**

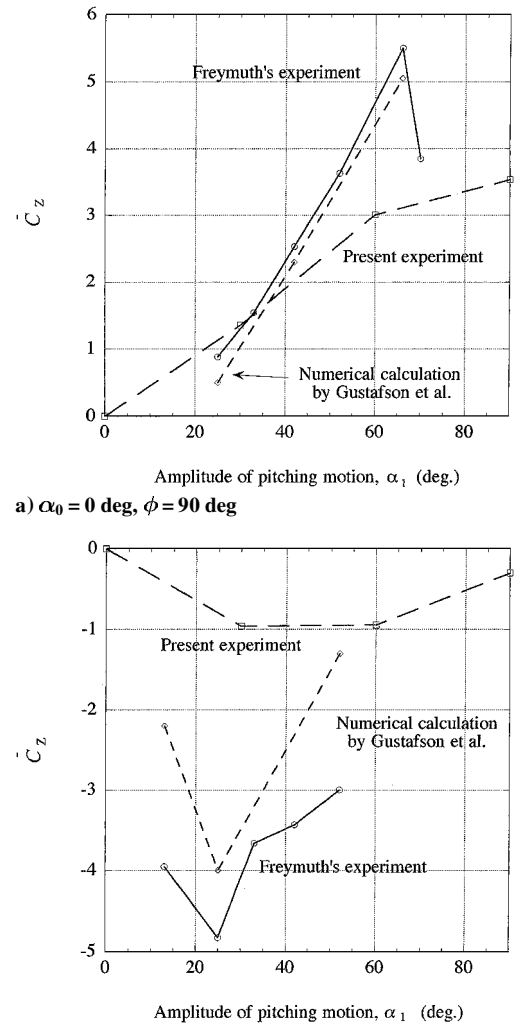


**Fig. 7 Comparison between our measurement results, the experimental results by Freymuth,[10] and the analytical results by Gustafson et al.[12,13]**

**Table 3 Comparisons between present experiments, experiments by Freymuth,[10] and numerical calculations by Gustafson et al.[12,13]**

| Parameter | Present experiments | Freymuth[10] experiments | Gustafson et al.[12,13] calculations |
|---|---|---|---|
| Airfoil shape | Rectangle, 5% thickness | Rectangle, 6.7% thickness, round edges | Ellipse, 15% thickness |
| Averaged airfoil/wing thickness,% | 5 | 6.2 | 23.5 |
| *Re* | $10^3$ | $1.7 \times 10^3$ | $1.7 \times 10^3$ |
| Planform | Rectangle, $AR = 10$ | Rectangle, $AR = 12$ | Two dimensional |

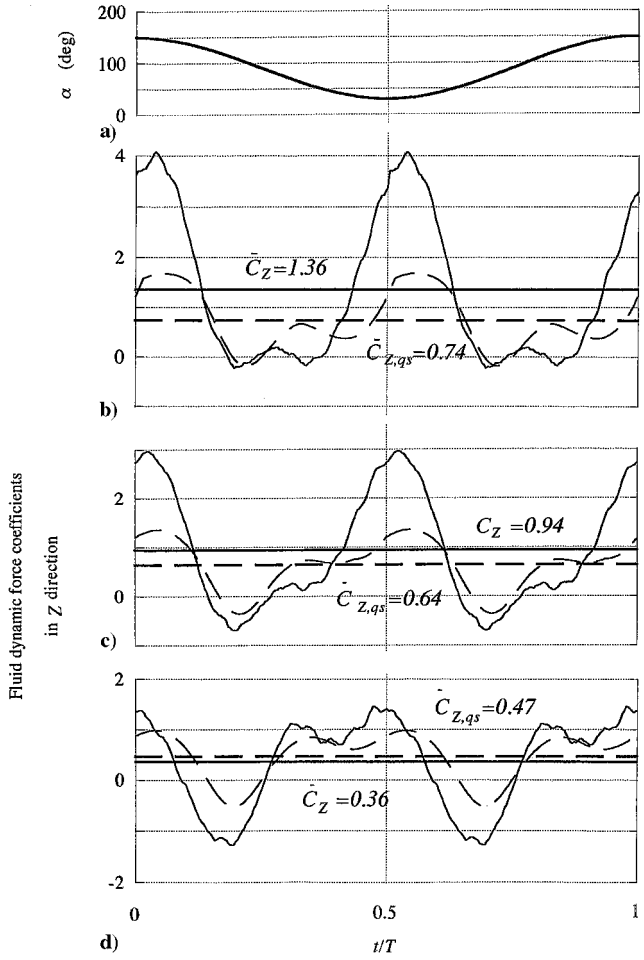


**Fig. 8 Time variations of force coefficients in the Z direction, $C_Z$ (——) and $C_{Z,qs}$ (- - -), and their averaged values, $\bar{C}_Z$ (——) and $\bar{C}_{Z,qs}$ (- - -), when $\alpha_0 = 90$ deg, $\alpha_1 = 60$ deg, and $\phi = -90$ deg: a) time variation of $\alpha$, b) $a = -0.5$, c) $a = 0$, and d) $a = 0.5$.**

Figure 8 shows our results for the wing motion of $\alpha_0 = 90$ deg, $\alpha_1 = 60$ deg, and $\phi = -90$ deg. Freymuth[10] called this type of wing motion mode 2 hovering. Figure 8a shows the time variation of $\alpha$, and Fig. 4a shows that of $X/h_0 = -h/h_0$ for this wing motion. Figures 8b, 8c, and 8d show the time variations of $C_Z$ (solid line) and $C_{Z,qs}$ (broken line) when $a = -0.5$, 0, and 0.5, respectively. The time-averaged values of $C_Z$ and $C_{Z,qs}$, that is $\bar{C}_Z$ (solid line) and $\bar{C}_{Z,qs}$ (broken line), are also shown in Figs. 8b–8d. In all of the wing motions in our present experiments, the wing motion when $a = -0.5$ is the closest to the wing motion of a real insect.[15] When Figs. 8b–8d are compared, the time-averaged thrust coefficient $\bar{C}_Z$ for this motion increased as $a$ decreased:

$$\bar{C}_Z = \begin{cases} 1.36, & \text{for} \quad a = -0.5 \\ 0.94, & \text{for} \quad a = 0 \\ 0.36, & \text{for} \quad a = 0.5 \end{cases} \tag{24}$$

This suggests that the pitching axis of an insect wing, which is at the leading edge, increases the time-averaged thrust $\bar{C}_Z$. This increase is also predicted by the potential flow theory,[15,18] where uniform flow is close to 0 and $k$ is close to $\infty$.

For all three values of $a$ (Figs. 8b–8d), the values of $C_Z$ differ from those of $C_{Z,qs}$. This difference indicates that the quasi-steady assumption is inadequate for analysis of these motions.

Figures 9a, 9b, and 9c show the flow around the wing for the wing motions in Figs. 8b, 8c, and 8d, respectively. The following equations are satisfied for these wing motions:

$$h(t/T = p) = -h\left(t\Big/T = \tfrac{1}{2} + p\right)$$

$$\alpha(t/T = p) + \alpha\left(t\Big/T = \tfrac{1}{2} + p\right) = 180\,\text{deg}, \quad 0 \le p \le \tfrac{1}{2} \tag{25}$$

The wing motion is symmetrical about the $Z$ axis, and the flow around the wing at $t/T = \frac{1}{2} + p$ is the same as that at $t/T = p$. In Figs. 9a–9c, the averaged induced flow in the $-Z$ direction agrees with the direction predicted by $\bar{C}_Z$ and simple momentum theory.

When $a = 0$ (Fig. 9b), vortex 1 is generated at $t/T \simeq \frac{7}{8}$ and then travels along surface 1 during $\frac{7}{8} \to t/T \to \frac{3}{8}$. At $t/T \simeq \frac{3}{8}$, vortex 1, which is close to edge B, induces flow from surface 1 toward surface 2. This flow generates vortex 2 on surface 2. At this moment, vortex 1′ is generated from edge A and coincides with the generation of vortex 1 at $t/T \simeq \frac{7}{8}$.

Compared with vortex 1 in Fig. 9b, the generation of vortex 1 when $a = -0.5$ (Fig. 9a) is delayed; it is generated at $t/T \simeq 0$ and then travels along surface 1 during $0 \to t/T \to \frac{3}{8}$. When $a = 0.5$ (Fig. 9c), the separated vortex 1 is generated at $t/T \simeq \frac{1}{8}$. At $t/T \simeq \frac{1}{4}$, vortex 2 is generated close to vortex 1. At $t/T \simeq \frac{3}{8}$, vortex 4 is generated instead of vortices 1 and 2, and vortex 3 is generated from edge A. Vortex 3 does not travel along the wing surface, but separates from the wing. Therefore, vortex 3 is not observed near the wing at $t/T \simeq \frac{1}{2}$.

The $C_Z$ is much higher than the $C_{Z,qs}$ near $t/T \simeq 0$ or $\frac{1}{2}$ in Figs. 8b and 8c ($C_Z/C_{Z,qs} > 2$). Figures 9a and 9b show the separated vortex 1 or 1′ at these moments. On the other hand, a vortex is not observed at $t/T \simeq 0$ or $t/T \simeq \frac{1}{2}$ in Fig. 9c, and the $C_Z$ is not much larger than the $C_{Z,qs}$ in Fig. 8d. Therefore, the large values of $C_Z$ near $t/T \simeq 0$ or $t/T \simeq \frac{1}{2}$ in Figs. 8a and 8b are strongly related to the vortex 1 or 1′. Dickenson and Götz[8] proposed the mechanism of high lift enhanced by a vortex, that is, vortex capture. Vortex capture is the phenomenon where a vortex generated during rotation is attached to a wing surface during the subsequent plunging motion. In Figs. 9a and 9b, vortex 1 (or 1′), which was generated by both plunging and pitching motions, remained on the wing surface until the plunging motion was stopped. Therefore, this behavior of vortex 1 or 1′ is similar to vortex capture.

Figure 10 shows the results for $\alpha_0 = 0$ deg, $\alpha_1 = 60$ deg, $\phi = 90$ deg, and $a = 0$. Freymuth[10] called this type of wing motion mode 1 hovering. Figure 10a shows the time variations of $\alpha$. Figure 4a shows the time variation of $X/h_0 = -h/h_0$. Figure 10b shows the time variation of $C_Z$ (solid line) and $C_{Z,qs}$ (broken line) and their time-averaged values, $\bar{C}_Z$ (solid line) and $\bar{C}_{Z,qs}$ (broken line). Similar to the wing motions of $\alpha_0 = 90$ deg, $\alpha_1 = 60$ deg, and $\phi = -90$ deg, the time variation of $C_Z$ differs from that of $C_{Z,qs}$, and $\bar{C}_Z$ differs from $\bar{C}_{Z,qs}$. These differences indicate that the quasi-steady assumption is inadequate for analysis of this wing motion.

Figure 10c shows the flow around the wing. The flow around the wing at $t/T = \frac{1}{2} + p (0 \le p \le \frac{1}{2})$ is the same as that at $t/T = p$ because of Eq. (25). In Fig. 10c, the averaged induced flow is in the $-Z$ direction, which agrees with the direction predicted by $\bar{C}_Z$ and simple momentum theory. Vortex 1 is generated at $t/T \simeq 0$ and then moves from edge A toward edge B along surface 1, and remains near edge B at $t/T \simeq \frac{1}{4}$. At $t/T \simeq \frac{1}{4}$, vortices 3 and 4 also exist on surface

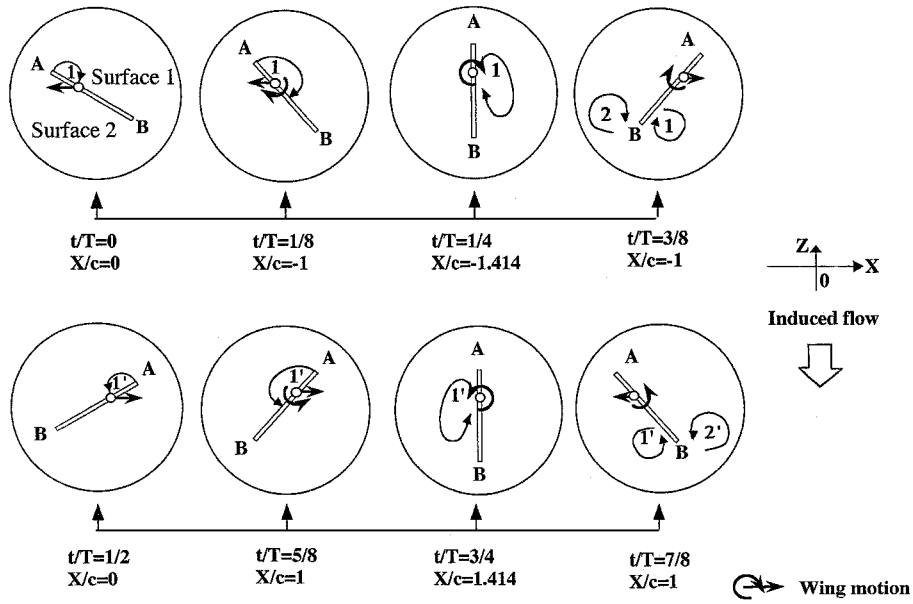


a) $a = -0.5$

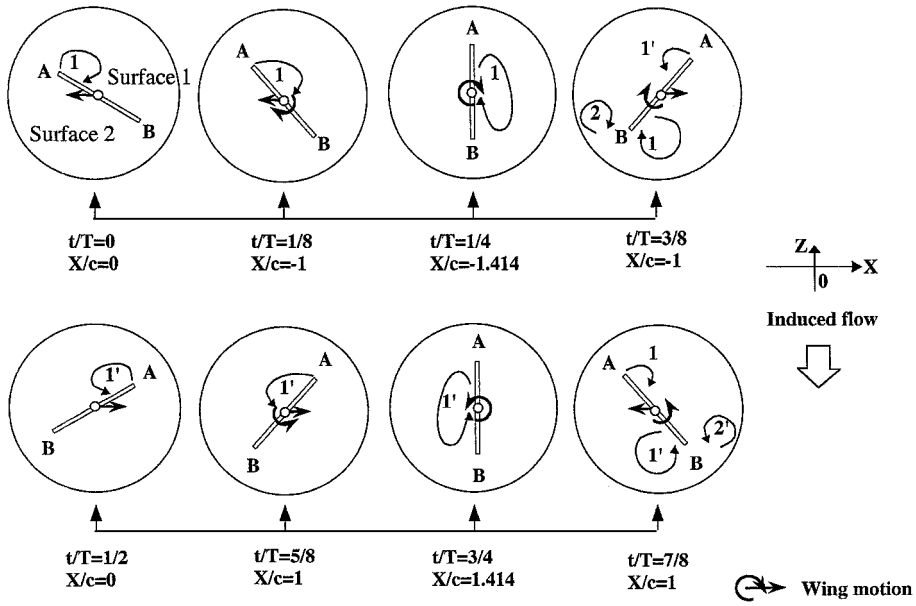


b) $a = 0$

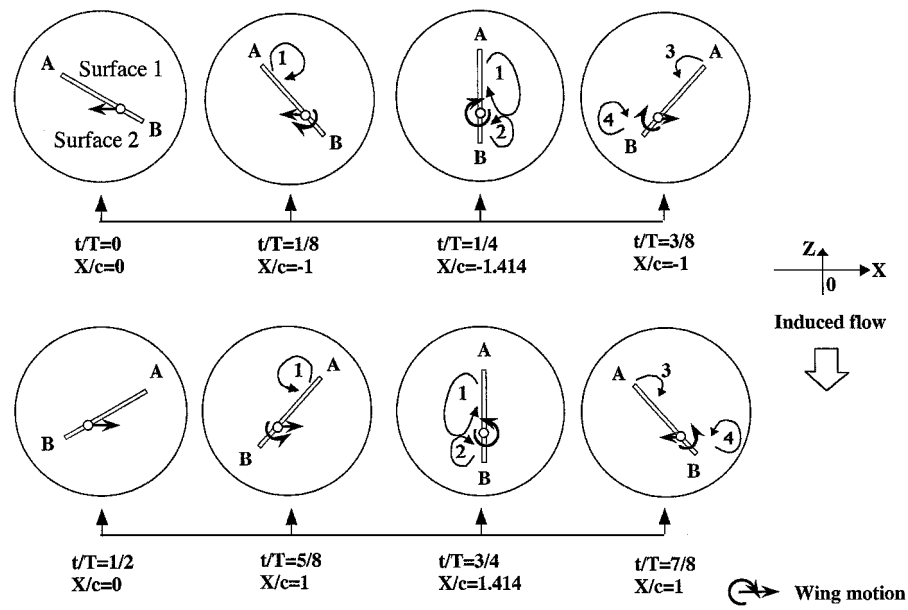


c) $a = 0.5$

**Fig. 9 Vortices generated from the wing whose motion is $\alpha_0 = 90$ deg, $\alpha_1 = 60$ deg, and $\phi = -90$ deg.**

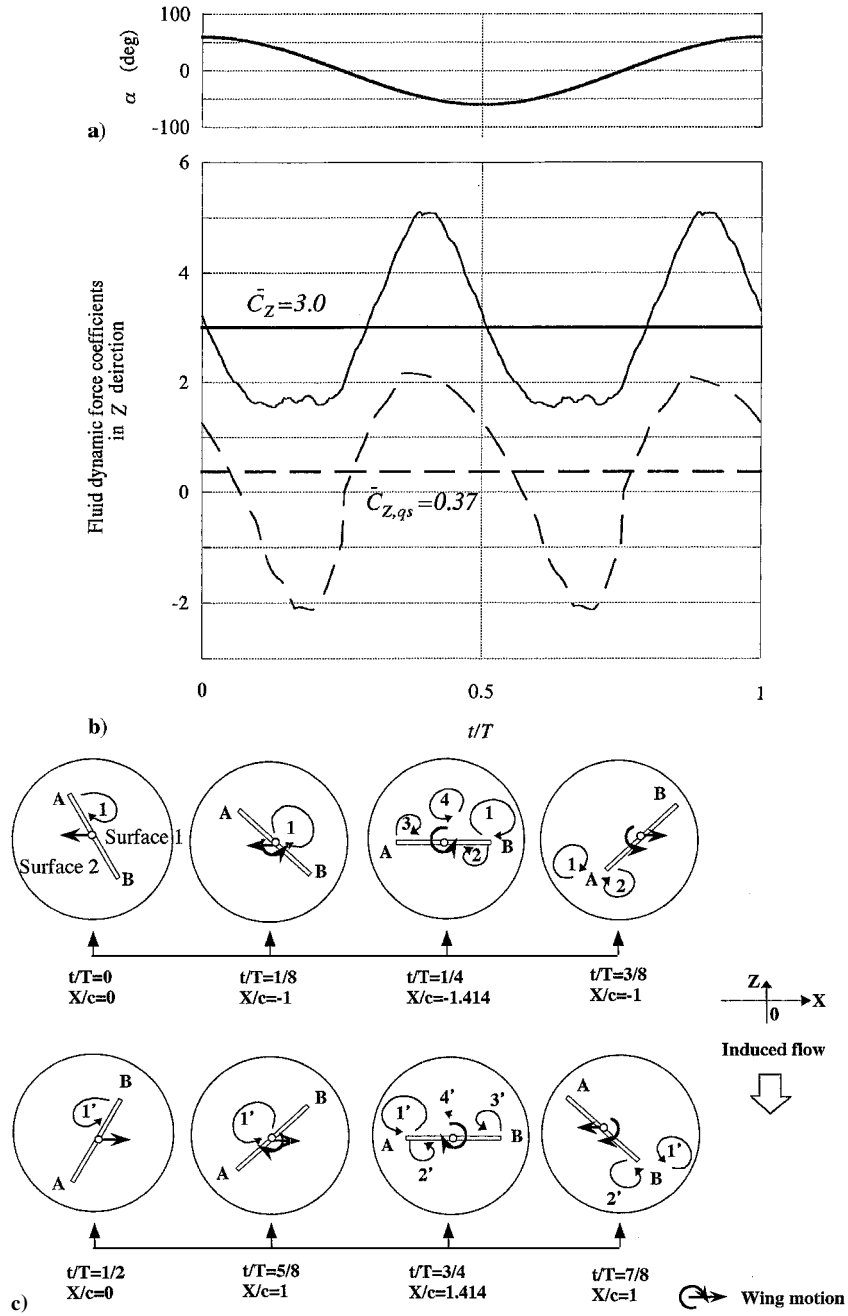


**Fig. 10 Time variation of force coefficients and flow around the wing when $\alpha_0 = 0$ deg, $\alpha_1 = 60$ deg, $\phi = 90$ deg, and $a = 0$: a) time variation of $\alpha$; b) time variations of force coefficients in the $Z$ direction, $C_Z$ (——) and $C_{Z_1qs}$ (– – –), and their averaged values, $\bar{C}_Z$ (——) and $\bar{C}_{Z_1qs}$ (– – –); and c) vortices generated from the wing.**

1, and vortex 2 is generated on surface 2. At $t/T \simeq \frac{3}{8}$, only vortices 1 and 2 are close to edge A, and vortices 3 and 4 are separated from the wing. The behaviors of these vortices generate $C_Z$, which is always larger than $C_{Z,qs}$, shown in Fig. 10b.

## Conclusions

The fluid dynamic forces acting on a wing during plunging and pitching motions [defined by Eq. (1)] were measured. The Reynolds number for this wing was $10^3$, and the reduced frequency was 0.35 [based on Eq. (2)]. In the analysis of the measured data, both the three-dimensional effect due to the finite value of $b/c$ on the fluid dynamic forces acting on the wing and the effect of the wave on the water surface on them were ignored. Furthermore, in the estimate of the efficiency $\eta$, only power for plunging motion was considered, and power for pitching motion was ignored. The following results were obtained from the analysis of the measured data:

1) The maximum time-averaged thrust $\bar{C}_Z$ occurred when the pitching axis was at the 25% chordwise position, that is, $a = -0.5$, $\alpha_0 = \alpha_1 = 90$ deg, and $\phi = 0$ deg. The maximum value of $\bar{C}_Z$ was about 4. Efficiency for this wing motion was fairly high ($\eta \simeq 0.8$), thus making this wing motion relevant in developing small-scale fluid machinery.

2) The maximum efficiency $\eta$ occurred when the pitching axis is at the 25% chordwise position, that is, $a = -0.5$, $\alpha_0 = \alpha_1 = 90$ deg, and $\phi = 45$ deg. The time-averaged thrust for this wing motion was also fairly high ($\bar{C}_Z \simeq 3$), thus making this wing motion relevant to the development of small-scale fluid machinery. Here we excluded the wing motions for $\alpha_0 = \alpha_1 = 90$ deg and $\phi = \pm 90$ deg because the efficiency could not be estimated with high accuracy. However, the exclusion of these wing motions is not a serious problem because these motions, whose time-averaged thrust is small ($\bar{C}_Z \simeq 0.5$), are not relevant to small-scale fluid machinery.

The measured fluid dynamic forces were larger than those estimated by quasi-steady analysis of the wing motion for $a = -0.5$, $\alpha_0 = 90$ deg, $\alpha_1 = 60$ deg, and $\phi = -90$ deg, which is close to the wing motion of real insects. These larger fluid dynamic forces are strongly related to vortex capture.[8] The time-averaged thrust coefficient $\bar{C}_Z$ was about 1.4, and the efficiency $\eta$ was about 0.4 for this

wing motion. Neither value is relatively high. The wing motion of an insect such as a dragonfly, which is a motion that is relatively common among flights of various forward speeds,[15] might be determined for maximizing flight performance of a cruising flight of the insect.

## Appendix: Steady Characteristics of a Wing

The lift and drag forces acting on a wing moving at a constant velocity $U = 0.17$ m/s for a fixed angle of attack $\alpha$, $F_Z(\alpha)$, and $F_X(\alpha)$ were measured. The Reynolds number $Re = Uc/\nu$ was $4 \times 10^3$. The coefficients $C_\ell(\alpha)$ and $C_d(\alpha)$ were obtained by

$$C_\ell(\alpha) = F_Z(\alpha) \Big/ \left(\tfrac{1}{2}\rho U^2 bc\right), \qquad C_d(\alpha) = F_X(\alpha) \Big/ \left(\tfrac{1}{2}\rho U^2 bc\right) \tag{A1}$$

These coefficients are shown in Fig. A1.

The Reynolds number in this measurement for a wing in steady motion is close to $Re = 10^3$, which is the Reynolds number indicated by Eq. (2). The steady characteristics obtained here were used in the quasi-steady analysis for a wing undergoing unsteady motion.

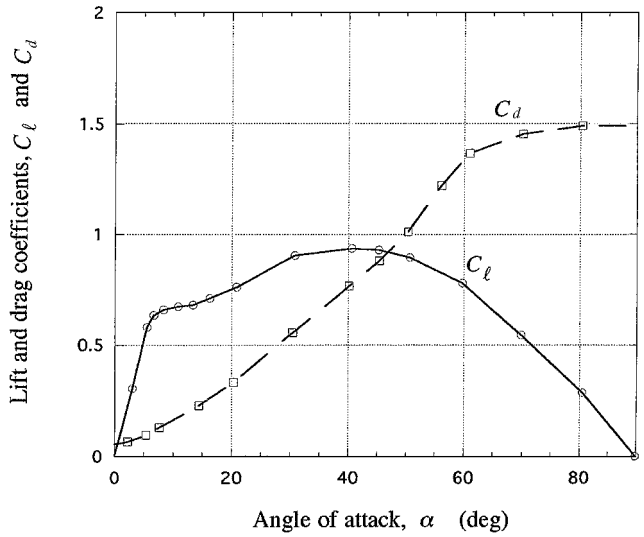


**Fig. A1 Steady characteristics of a flat rectangular plate with 5% thickness at $Re = 4 \times 10^3$.**

## Acknowledgment

This research is supported by Research and Development Applying Advanced Computational Science and Technology, Japan Science and Technology.

## References

[1]Weis-Fogh, T., "Quick Estimates of Flight Fitness in Hovering Animals, Including Novel Mechanisms for Lift Production," *Journal of Experimental Biology*, Vol. 59, 1973, pp. 169–230.

[2]Bisplinghoff, R. L., Ashley, H., and Halfman, R. L., *Aeroelasticity*, Addison–Wesley, Reading, MA, 1955, Chap. 5.

[3]Norberg, R. A., "Hovering Flight of the Dragonfly *Aeschna Juncea L.*, Kinematics and Aerodynamics," *Swimming and Flying in Nature*, Vol. 2, Plenum, New York, 1975, pp. 763–781.

[4]Somps, C., and Luttges, M.,"Dragonfly Flight: Novel Uses of Unsteady Separated Flows," *Science*, Vol. 26, June 1984, pp. 1326–1329.

[5]Reavis, M. A., and Luttges, M. W., "Aerodynamic Forces Produced by a Dragonfly," AIAA Paper 88-0330, 1988.

[6]Ellington, C. P., van Den Berg, W. A. P., and Thomas, A. L. R., "Leading-Edge Vortices in Insect Flight," *Nature*, Vol. 384, 1996, pp. 626–630.

[7]Dickinson, M. H.,"Wing Rotation and the Aerodynamic Basis of Insect Flight," *Science*, Vol. 284, 1999, pp. 1954–1960.

[8]Dickinson, M. H., and Götz, K. G., "Unsteady Aerodynamic Performance of Model Wings at Low Reynolds Numbers," *Journal of Experimental Biology*, Vol. 174, 1993, pp. 45–64.

[9]Dickinson, M. H., "The Effects of Wing Rotation on Unsteady Aerodynamic Performance at Low Reynolds Numbers," *Journal of Experimental Biology*, Vol. 192, 1994, pp. 179–206.

[10]Freymuth, P., "Thrust Generation by an Airfoil in Hover Modes," *Experiments in Fluids*, Vol. 9, 1990, pp. 17–24.

[11]Gustafson, K., and Leben, R., "Computation of Dragonfly Aerodynamics," *Computer Physics Communications*, Vol. 65, 1991, pp. 121–132.

[12]Gustafson, K., Jones, K., Leben, R., and McArthur, J., "Vortex Patterns Thrust and Lift for Hovering Modes," *Proceedings of the 4th International Symposium on Computational Fluid Dynamics*, Davis, CA, 1991, pp. 461–466.

[13]Gustafson, K., Leben, R., and McArthur, J., "Lift and Thrust Generation by an Airfoil in Hover Modes," *Computational Fluid Dynamics Journal*, Vol. 1, No. 1, 1992, pp. 47–57.

[14]Freymuth, P., Finaish, Finaish, and Bank, W., "Three-Dimensional Vortex Patterns in a Starting Flow," *Journal of Fluids Mechanics*, Vol. 161, 1985, pp. 239–248.

[15]Azuma, A., *The Biokinetics of Flying and Swimming*, Springer-Verlag, Tokyo, 1992, Chap. 4.

[16]Johnson, W., *Helicopter Theory*, Dover, New York, 1980, pp. 28–35.

[17]Sedov, L. I., *Two-Dimensional Problems in Fluid Dynamics and Aerodynamics*, Interscience, New York, 1965, pp. 20–30.

[18]Fung, Y. C., *An Introduction to the Theory of Aeroelasticity*, Wiley, London, 1955, Chap. 13.

P. R. Bandyopadhyay
*Associate Editor*